THE ASTROPHYSICAL JOURNAL, 452:693–703, 1995 October 20

DENSE GAS IN THE DR 21 REGION: HIGH-RESOLUTION IMAGING OF THE NH_3 INVERSION LINES

T. L. WILSON,[1] R. A. GAUME,[2,3] K. J. JOHNSTON,[2] AND A. R. TIEFTRUNK[1]
Received 1994 October 24; accepted 1995 April 26

ABSTRACT

Three arcsecond angular resolution images of the $(J, K) = (1, 1)$ and (3, 3) inversion lines of NH_3 toward the DR 21 H II region are presented. There is absorption in the (1, 1) line toward DR 21 and emission to the northwest, northeast, southwest, and south. The NH_3 region found in emission in the (1, 1) line southwest of DR 21 is likely the same cloud seen in absorption toward the H II region. If the emission and absorption regions are taken as one cloud, this is the most massive and largest near DR 21. In the $(J, K) = (1, 1)$ line this cloud shows a velocity gradient of 15 km s^{-1} pc^{-1}. To the northeast, low-brightness continuum emission extends over a larger region, and there is little NH_3. In the (1, 1) emission line, filament-like NH_3 emission regions are elongated N-S $> 20''$; for most, the emission is almost unresolved in the E-W direction. In most cases these filaments have a position angle that is very close to that measured for the molecular cloud over $> 10'$. The NH_3 emission line delineates the location of the denser molecular gas. The presence of dense clouds south and southwest of the continuum source and the sharp falloff of the H II continuum intensity to the southwest gives support to the notion that the expansion of the H II region is halted by dense neutral gas to the southwest.

The structures traced by the (3, 3) transition differ greatly from those found for the (1, 1) line. Toward the H II region DR 21, there are several (3, 3) emission maxima, two of which exhibit prominent negative velocity line wings. The (3, 3) line traces the hotter shocked gas. Given the negative velocity wings, the morphology of the (3, 3) line emission and the location of the NH_3 emission relative to the powerful outflow seen in vibrationally excited H_2 and other molecules, we conclude that the NH_3 represents the remnant material that has survived the powerful outflow. We estimate the location of the outflow source assuming that this is located near the shocked gas midway between the two NH_3 (3, 3) maxima with prominent negative velocity line wings.

Subject headings: H II regions — ISM: individual (DR 21) — ISM: kinematics and dynamics — ISM: molecules — radio lines: ISM

1. INTRODUCTION

Toward the southern end of the DR 21-W75S molecular cloud complex is the compact H II region DR 21. The molecular cloud extends over $> 20'$ with an axis approximately N-S (Morris et al. 1974; Bieging, Wilson, & Downes 1982; Wilson & Mauersberger 1990). The evolution of this complex appears to proceed from south to north; stars have already formed in the H II region DR 21, while to the north, the development is not so advanced (see, e.g., Garden & Carlstrom 1992). At radio and infrared wavelengths, DR 21 is one of the more luminous sources in the galaxy. The H II region itself consists of more than six compact components, A through F, whose free-free emission requires at least six O stars (Harris 1973). The DR 21 H II region is optically obscured, since it is behind most of the molecular gas, which has a column density of order 10^{23} cm^{-2} (Righini-Cohen, Simon, & Young 1979, if we use $1^m = 10^{21}$ cm^{-2}). There is an extraordinary outflow, in a roughly E-W direction, found in CO (Fisher et al. 1985), vibrationally excited H_2 (Garden et al. 1986), $C^{18}O$ (Wilson & Mauersberger 1990), and HCO^+ (Garden & Carlstrom 1992 and references therein). The interaction of this outflow with the parent molecular cloud has had a profound effect on the evolution of the region. The details of the interaction between newly formed stars and molecular clouds are not well understood; observational studies of molecular clouds during the early stages of massive star formation may lead to a better understanding of this process but require an angular resolution of better than a few arcseconds to match the resolutions obtained for infrared and continuum studies. Such resolutions are possible with the Very Large Array (VLA) in the inversion lines of NH_3.

It is generally accepted that NH_3 metastable $(J = K)$ emission lines are collisionally excited. For emission, the H_2 density needed for an effective collisional excitation, the critical density, is 3×10^4 cm^{-3} for NH_3 inversion lines. The metastable inversion lines are excellent interstellar thermometers (see, e.g., Danby et al. 1988). The (3, 3) levels are 123 K above the ground state, while the (1, 1) levels are 23 K above ground. Thus, differences in the spatial distributions of these lines are an indication of differences in kinetic temperature, T_k. The (3, 3) energy levels arise from ortho–NH_3, and the (1, 1) from para–NH_3. Since in the interstellar medium these forms are not interconverted easily, the excitation of these forms may be very different, and there may be no simple relation between the column densities. However, an approximate determination of T_k is possible; most importantly, the measurement of transitions arising from energy levels separated by nearly 100 K allows an estimate of T_k over a wide range.

From the point of view of NH_3 excitation, DR 21 is of great interest. Based on lower resolution single-dish observations, Wilson, Batrla, & Pauls (1982) and Guilloteau et al. (1983)

[1] Max-Planck-Institut für Radioastronomie, Postfach 2024, D-53010 Bonn, Germany.
[2] US Naval Observatory, 3450 Massachusetts Avenue NW, Washington, DC 20392-5420.
[3] Code 7213, Naval Research Laboratory, Washington, DC 20375-5351.

reported the detection of maser emission in the (3, 3) inversion line, and Matsakis et al. (1977) found maser emission in a (1, 1) satellite hyperfine component. Higher spatial resolution interferometric observations have been reported by Matsakis et al. (1981) for the (1, 1) transition and Guilloteau et al. (1983) for the (3, 3) transition. Both these observations suffered from rather high noise levels and produced limited results. Keto (1990) observed both the (1, 1) and (3, 3) transitions toward DR 21. The (1, 1) data were of moderate signal-to-noise ratio (S/N) (10 mJy beam^{-1}), but discussion of the (3, 3) data was limited because the noise level was a factor of 3 higher. Therefore, to understand the detailed interaction of outflow, H II region, and nearby molecular material better, we have imaged the NH_3 distribution in the (1, 1) and (3, 3) inversion lines with the VLA in the D configuration. We present the first images of the spatial distribution of the (3, 3) NH_3 transition toward DR 21 and images of the (1, 1) transition with higher S/N and better spatial resolution than previous observations.

2. OBSERVATIONS AND DATA REDUCTION

The observations were made in a single 6 hr session on 1992 September 17 using the VLA telescope of the National Radio Astronomy Observatory (NRAO).[4] At the time of the observations, the VLA was in the D configuration, which provides baseline lengths from 35 m to 1.03 km. Our observations are not sensitive to source structures larger than $\sim 60''$.

NH_3 in the DR 21 region was observed for a total on-source time of about 2.6 hr, divided between the (1, 1) inversion line (rest frequency 23694.496 MHz) and the (3, 3) inversion line (23870.130 MHz). The central pointing position for these observations was R.A. = $20^h37^m14^s.0$, decl. = $+42°09'08''$ (B1950.0). The source 3C 286 served as an absolute flux density calibrator; the flux density was assumed to be 2.44 Jy at the observing frequency. The source 2005+403 (2.4 Jy) was monitored frequently as a phase calibrator. 3C 84 was used as a bandpass calibrator.

The line observations were made in a VLA spectral line mode with a total bandwidth of 6.25 MHz, separated into 64 channels, with on-line Hanning weighting, providing a channel separation and spectral resolution of 97 kHz (1.24 km s^{-1}). Channel 32 was set to an LSR velocity of 0 km s^{-1}. The data were inspected, edited, and calibrated using the NRAO Astronomical Image Processing System (AIPS) software as implemented on NRL and USNO computer systems. To improve data quality, a self-calibration algorithm was applied to the wide-band channel 0 (continuum data). The improved antenna gain solutions derived from self-calibration were later applied to the entire spectral line data set.

The self-calibrated continuum data were Fourier-inverted using both "natural" and "uniform" weighting of the u, v data. Natural weighting of the u, v data results in greater overall sensitivity, and greater sensitivity to extended structure, with lower spatial resolution. The rms noise level and full width at half-maximum (FWHM) beam size of the continuum images resulting from natural weighting of the data are 1 mJy beam^{-1} and $3''.3$, respectively.

In order to obtain "line-only" images, a linear fit to the continuum was performed in the visibility plane using channels without line emission or absorption. For the (1, 1) transition, a total of 19 channels was used; for the (3, 3) transition, 16 channels were used. The fit was then subtracted from visibilities in all the channels to produce a line-only data set (Cornwell, Uson, & Haddad 1992). These data were then Fourier-inverted using natural weighting and CLEANed in the standard manner. To obtain the best sensitivity, we have used only naturally weighted data in the following analysis and discussion. The rms noise level and FWHM beam size for the spectral line images are 6.5 mJy beam^{-1} and $3''.3$, respectively. This is equivalent to a main beam brightness temperature of 0.2 K.

[4] The NRAO is operated by Associated Universities, Inc., under cooperative agreement with the National Science Foundation.

3. RESULTS AND DISCUSSION

3.1. *Continuum Structure*

In Figure 1 we show a contour plot of an image of the continuum structure of DR 21. We have labeled the continuum peaks following the convention used by Harris (1973). With $3''.3$ resolution, we find four distinct high-brightness peaks, B–E, and a fifth source, A, in the western shoulder of C. This result agrees very well with the maps of Harris (1973), Guilloteau et al. (1983), and Roelfsema, Goss, & Geballe (1989). We also detect the lower brightness, extended region to the east, found previously by Roelfsema et al. (1989). This region is labeled F in Figure 1. The overall extent is $> 1'$, in agreement with Roelfsema et al. (1989). The total flux density from our image is 14 Jy, 73% of the single-dish value. This result is in excellent agreement with Guilloteau et al. (1983). The peak main beam brightness temperature in the image is ≈ 400 K. Given that the electron temperature is 8400 K (Wilson, Bieging, & Wilson 1979), the peak continuum optical depth is less than 0.06. There is a very good agreement with the 3.5 mm continuum map of Garden & Carlstrom (1992). On this basis, there are no very intense components that become optically thin at wavelengths shortward of 1.3 cm. In Figure 1, we also show the location of the HCO^+ maximum nearest DR 21 found by Garden & Carlstrom (1992).

3.2. *The* NH_3 (1, 1) *Line Data*

The gray scale in Figure 1 depicts the velocity-integrated NH_3 (1, 1) line-to-continuum ratio for the deepest absorption, integrated over v_{LSR}'s from -3.7 km s^{-1} to 0 km s^{-1}. From the distribution of the line-to-continuum ratio, the NH_3 absorption is concentrated toward the southern part of continuum source. The largest line-to-continuum ratio is found slightly offset to the south of the peak continuum intensity. To the north and east the NH_3 (1, 1) line-to-continuum ratio is significantly less. Toward DR 21D, there is only a very small amount of molecular material covering the continuum.

In Figure 2*a*, we show a contour plot of the velocity-integrated NH_3 (1, 1) emission and absorption in DR 21. These zeroth-moment data were obtained by integrating the NH_3(1, 1) line data over a velocity range of -3.7 to 0.0 km s^{-1}. In addition to the absorption there are four emission regions, northwest (region 1), south (region 2), southwest (region 3), and northeast (region 4), relative to DR 21. Figures 2*b*–2*d* show contour plots of three of the NH_3 (1, 1) velocity channels covering the main hyperfine emission component. The properties of the emission regions are listed in Table 1. Contours of the NH_3 (1, 1) absorption seen in the -1.2 and 0.0 km s^{-1} velocity channels (Figs. 2*c* and 2*d*) make an abrupt transition to emission contours southwest of the continuum source. This NH_3 (1, 1) emission is close to the location of the HCO^+ maximum. We assume that this emission-line NH_3 cloud is on

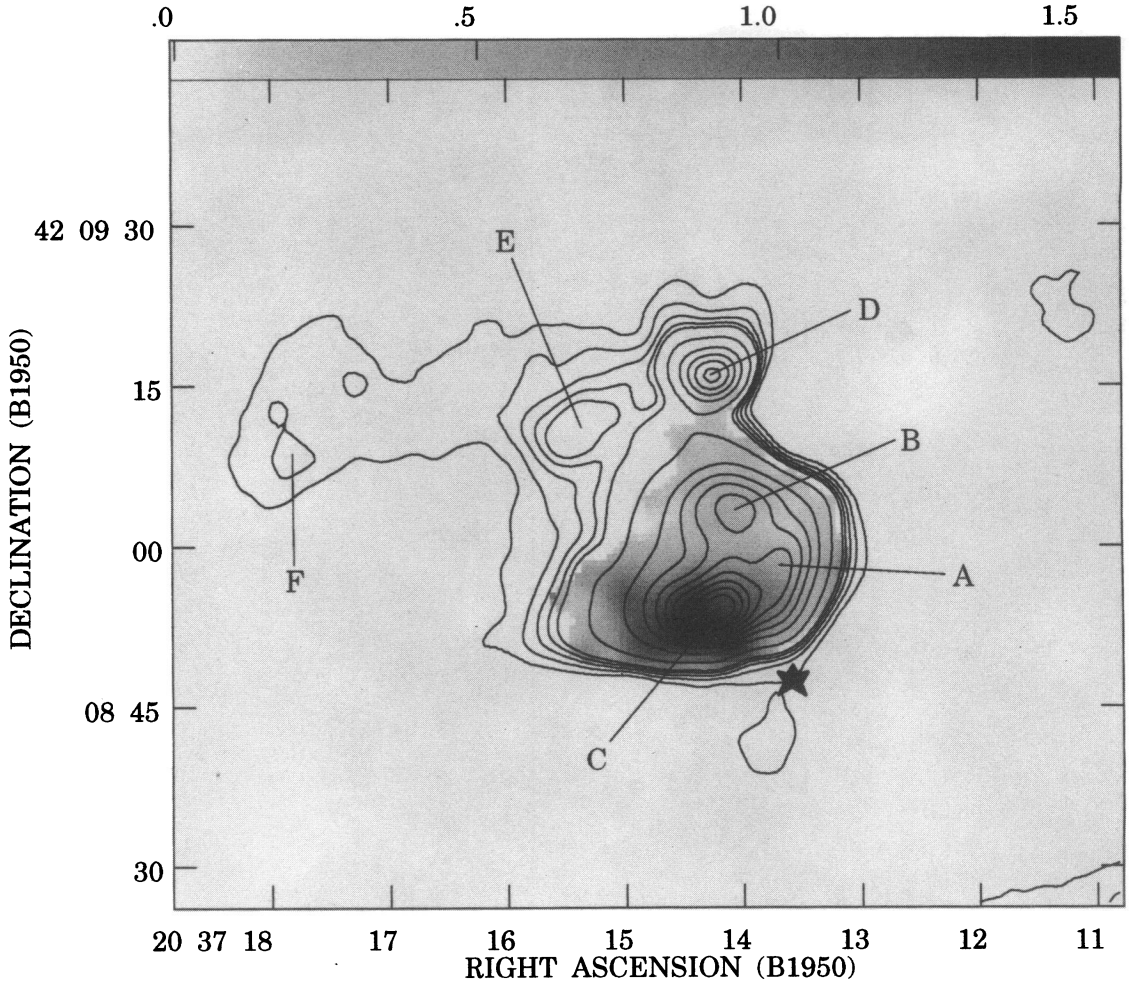

FIG. 1.—Continuum image of DR 21 at a wavelength of 1.3 cm displayed in contours. The continuum image was produced by a Fourier inversion of naturally weighted u, v data, with a FWHM beam size of 3".3. This image is corrected for primary beam taper. We have labeled the various continuum peaks following Harris (1973) and Roelfsema et al. (1989). The peak intensity is 1.257 Jy beam^{-1}, and contours are 1, 2, 3, 4, 5, 10, 20, 30, 40, 50, 60, 70, 80, and 90% of this value. The gray scale represents the velocity-integrated NH_3 (1, 1) line-to-continuum absorption ratio. The absorption profile was integrated over the main (1, 1) hyperfine transition in a velocity range of -3.7 to 0.0 km s^{-1}. The values of the gray scale range from 0 to 1.56 km s^{-1}. The star, southwest of source C, marks the location of the HCO^+ maximum closest to DR 21 (Garden & Carlstrom 1992).

the near side of the H II region and is part of the same cloud seen in absorption against the H II region. The emission-line regions in the south and southwest are close to those portions of the H II region in which there is a rapid falloff in the continuum intensity. From Roelfsema et al. (1989) and our Figure 1, to the east there is a lower brightness region of ionized gas (labeled F in Fig. 1). The molecular line and continuum data give strong support for a picture in which the expansion of the H II region is halted by the presence of dense molecular gas in the southwest. In the west, DR 21 is ionization bound (all ionizing stellar photons are absorbed). To the east, the presence of lower brightness, more extended ionized gas indicates that free expansion is taking place. Here, the H II region is density bound (stellar ionizing photons escape). Regions 2 and 3, south of DR 21, are elongated in a roughly N-S direction. The sizes listed in Table 1 have been obtained from the geometric means, after deconvolution assuming Gaussian beam and source shapes. Region 1, to the northwest, is more irregu-

TABLE 1

PROPERTIES OF THE NH_3 $(J, K) = (1, 1)$ EMISSION-LINE REGIONS

Region	α	δ	Optical Depth	Linewidth[a] (Δv_{LSR} km s^{-1})	FWHP Size	Diameter (pc)	Mass ($M_\odot$)
1	$20^h37^m12^s.5$	+42°09′16″	≈ 1.7	2.4	≈ 20	≈ 0.2	≈ 100
2	20 37 14.8	+42 08 40	≈ 2.2	1.2	≈ 10	≈ 0.1	< 15
3	20 37 13.5	+42 08 42	≈ 1.5	2.4	≈ 20	≈ 0.2	≈ 100
4	20 37 15.4	+42 09 18	≈ 1	1.2	< 10	< 0.1	< 15

[a] Includes instrumental resolution of 1.2 km s^{-1}.

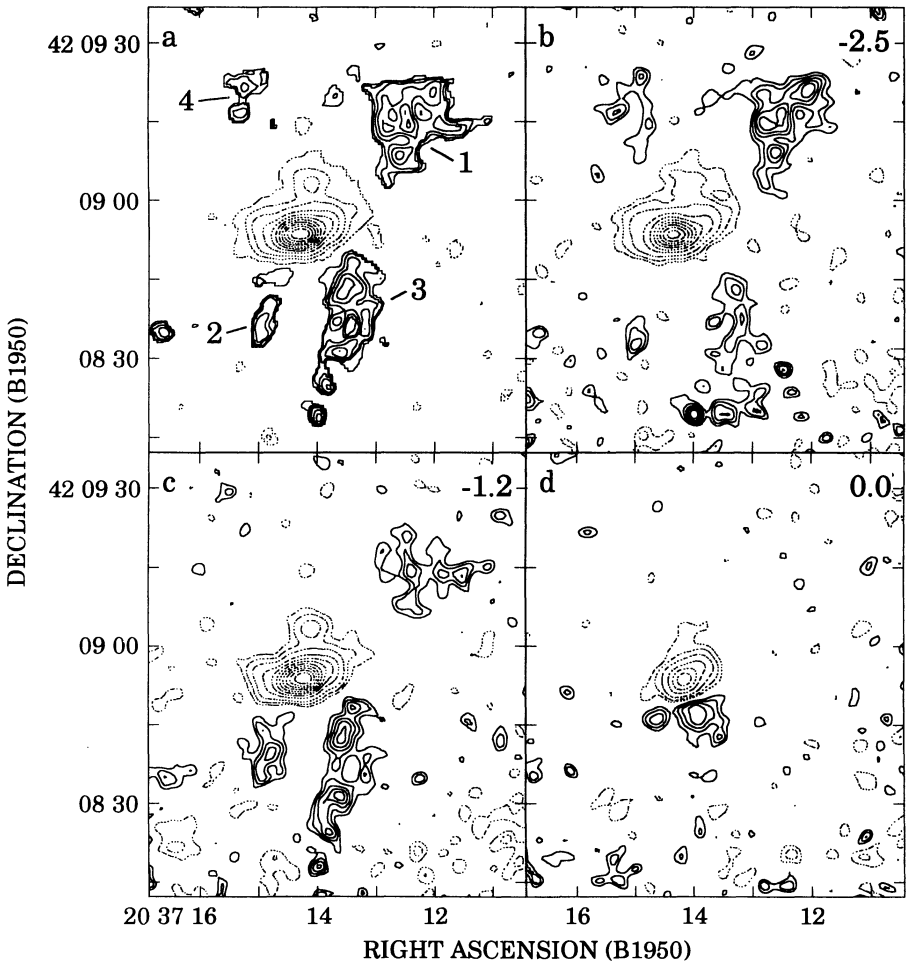

FIG. 2.—(*a*) Contour plot of the velocity-integrated NH_3 (1, 1) line intensities, integrated from -3.7 km s^{-1} to 0.0 km s^{-1}. Positive contours are shown as solid lines, and negative contours are shown as dashed lines. The emission-line regions are labeled 1–4. Parameters for these sources are given in Table 1. All spectral line images have been corrected for primary beam taper. The contour levels are -90, -80, -70, -60, -50, -40, -30, -20, -10, -5, -1, 1, 2, 3, 4, 5, and 6% of 1.715 Jy beam^{-1} km s^{-1}. (*b–d*) Plots of channels for $v_{LSR} = -2.5$, -1.2, and 0.0 km s^{-1}. Contour levels are -90, -80, -70, -60, -50, -40, -30, -20, -10, -5, -2.5, 2.5, 3.5, 4.5, 5.5, and 6.5% of 765 mJy beam^{-1}.

lar. There is a change in v_{LSR} of 1.2 km s^{-1} in region 3 in a roughly N-S direction. This motion is similar to rotation, but the irregularity of the region and our rather low velocity resolution indicate that caution should be used in drawing conclusions.

In Figure 3, we show spectra for the integrated (1, 1) emission-line maxima and for the absorption-line data. The emission maxima are labeled 1, 2, 3, and 4 as in Figure 2*a*. We assume that the wider emission pedestals seen in the spectra for regions 2 and 3 centered at $\sim v_{LSR} = 10$ km s^{-1} are instrumental. The line emission and absorption were integrated over irregularly shaped spatial regions determined from the zeroth-moment image (Fig. 2*a*). From Figure 3, in the (1, 1) line, the absorption and emission regions have about the same v_{LSR}. From the line widths and sizes, virial masses have been estimated assuming that pressure and magnetic effects can be neglected compared to self-gravity. These are listed in Table 1. Compared to single-dish results (Wilson & Mauersberger 1990), our NH_3 absorption-line spectrum (Fig. 3) is significantly deeper. This is because the 40″ beam of the 100 m telescope blends the emission and absorption regions, whereas these are well separated with the 3″ resolution of the VLA data. A fit to the outermost hyperfine components will not lead to very useful results because of the deviations from local thermodynamic equilibrium (LTE). These deviations are less pronounced for the inner hyperfine components, however, and allow an estimate of the optical depth of the (1, 1) line. We obtain $\tau = 2$, which is considerably larger than the apparent optical depth, 0.2, which can be obtained from the single-dish data of Wilson & Mauersberger (1990). From the ratio of our line-to-continuum data in Figure 1, it appears that $\sim$20% of the continuum is covered by the NH_3, which reconciles the values of apparent optical depth from T_l/T_c and the optical depth obtained from the hyperfine ratio. In addition to the absorption lines, Wilson & Mauersberger (1990), with a 40″ beam, detected an NH_3 emission component toward the continuum source. We do not find this in the VLA spectrum and conclude that the emission seen with the single dish was caused by a cloud or clouds in the edge of the beam, away from the continuum source, that is, regions 1–4. Combining our VLA optical depth estimates with a value of $T_k = 27$ K from the single-dish spectral line data, we find a total NH_3 column density of 3×10^{15} cm^{-2}. The $C^{18}O$ $J = 2$–1 line data of Wilson & Mauersberger (1990) give the same v_{LSR} as the NH_3 data, but the line width is 2 times larger. From the $C^{18}O$-$N(H_2)$ relation of Mauersberger et al. (1992), we find an H_2

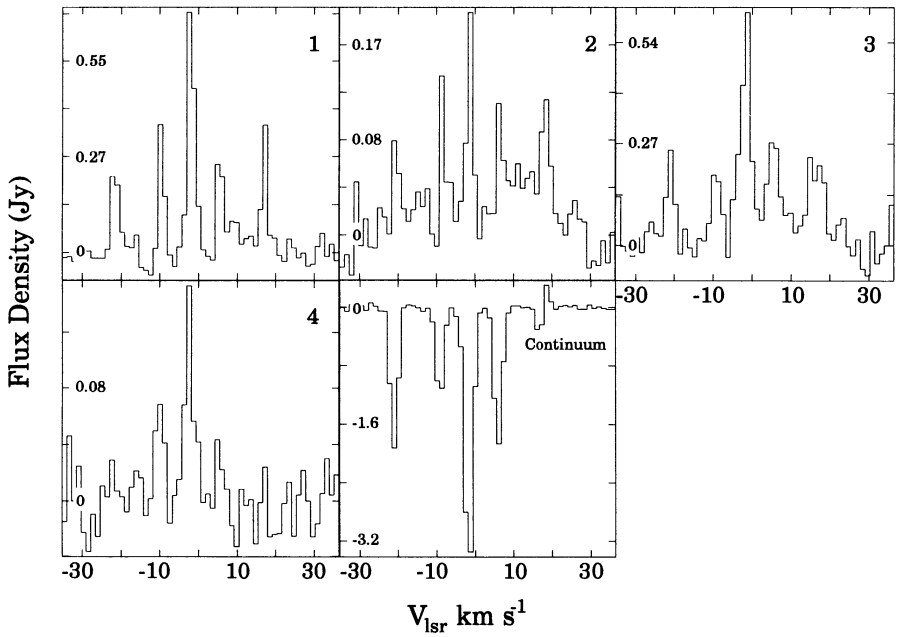

FIG. 3.—Spatially integrated spectra of the NH_3 (1, 1) inversion line toward emission-line regions 1, 2, 3, and 4, and the absorption toward the continuum H II region (see Fig. 2*a*). The irregularly shaped regions used for the spatial integrations were chosen from the zeroth-moment image (Fig. 2*a*). Line parameters for the four emission regions are given in Table 1.

column density of 1.3×10^{23} cm^{-2}. The $C^{18}O$ data were taken toward the peak of the continuum, so we associate this with the absorption. This result is supported by estimates of extinction based on near-IR data (Righini-Cohen et al. 1979). If we combine the H_2 column density with the NH_3 column density from the absorption-line data, we obtain an NH_3/H_2 ratio of 10^{-8}. This is about the ratio found in moderately dense regions. From a comparison of $C^{18}O$ toward the continuum peak with regions more than 45″ away, we find that the $C^{18}O$ is blueshifted by more than 0.5 km s^{-1}. The emission from our region 3 directly adjoins the absorption. This indicates that nearly all of this molecular gas must be in front of the H II region. The more positive v_{LSR} of the H II gas indicates that there is a flow off the foreground cloud.

Of the four emission sources, region 3 is the most interesting. This clump is prominent in the 13″ resolution $J = 1$–0 line map of HCN (Dickel, Ho, & Wright 1985) and the 10″ resolution $J = 1$–0 line map of HCO^+ (see our Fig. 1; Garden & Carlstrom 1992). The positions of these maxima agree with the position of our region 3, as do mass estimates based on the virial theorem. However, Dickel et al. (1985) reported that the most intense HCN emission has $v_{LSR} = -5$ km s^{-1}, whereas our results show emission and absorption between -3.7 km s^{-1} and 0 km s^{-1}. These velocity differences may be caused by large optical depths and self-absorption in the $J = 1$–0 line of HCN. If so, the physical parameters based on HCN data are open to question; HCN observations with higher velocity resolution are needed to check this hypothesis. Alternatively, the HCN may arise in a foreground cloud that is closer to the outflow and is more blueshifted. In any event, region 3, with a mass of 100 $M_\odot$, along with region 1 are definitely the most massive emission-line molecular clouds seen in NH_3 close to DR 21; however, there is considerably more molecular material near DR 21, since from $C^{18}O$ data taken with a 12″ resolution, Wilson & Mauersberger (1990) find a cloud with a FWHP extent of 1′ and FWHP line width of 3.6 km s^{-1}. From the virial theorem, this cloud has a molecular mass of 2300 $M_\odot$. From the integrated $C^{18}O$ $J = 2$–1 line emission, the total molecular mass is 5000 $M_\odot$. From the virial mass and cloud size, the average density of this cloud is about 4×10^4 cm^{-3}. Even if the uncertainties are of order 2, the NH_3 and HCN interferometric data record less than 20% of the mass. The other regions seen in NH_3 contribute only a small mass: for region 2, <15 $M_\odot$, and the mass of region 4 is probably also small.

To investigate dynamics, we show position-velocity plots in Figure 4. On the basis of similar position-velocity diagrams, Keto (1990) had reported finding radial motions in two clouds, the first with a position close to our region 3, south of DR 21, and the second close to our region 1, northwest of DR 21. In both cases, Keto (1990) concluded that the clouds are contracting. In order to test this hypothesis using our higher spatial resolution and higher S/N data, we have constructed right ascension–velocity and declination-velocity diagrams using the same positions, radial velocity intervals, and contour levels as Keto (1990). The right ascension–velocity diagram, Figure 4*a*, is for the more southerly declination. This shows emission from regions 2 and 3, with main and inner satellite hyperfine components. The accompanying declination-velocity diagram, Figure 4*b*, shows two interesting features. First, there is prominent absorption toward the continuum source. This is found for hyperfine components at v_{LSR}'s -19, ± 8, and 0 km s^{-1}, but *not* at $+19$ km s^{-1}, where the hyperfine satellite is found as a weak emission feature. This non-LTE effect is explained by noncontracting line-leaking models of the type proposed by Matsakis et al. (1977). Second, there is a slight trend for the main hyperfine component to move to positive v_{LSR}'s between declination = 42°08′20″ and 50″. Figures 4*c* and 4*d* show position-velocity plots covering NH_3 emission region 1. Emission is seen from both the main and inner satellite hyperfine components. There are apparently no significant velocity shifts or gradients in region 1. The arclike features seen in the plots of

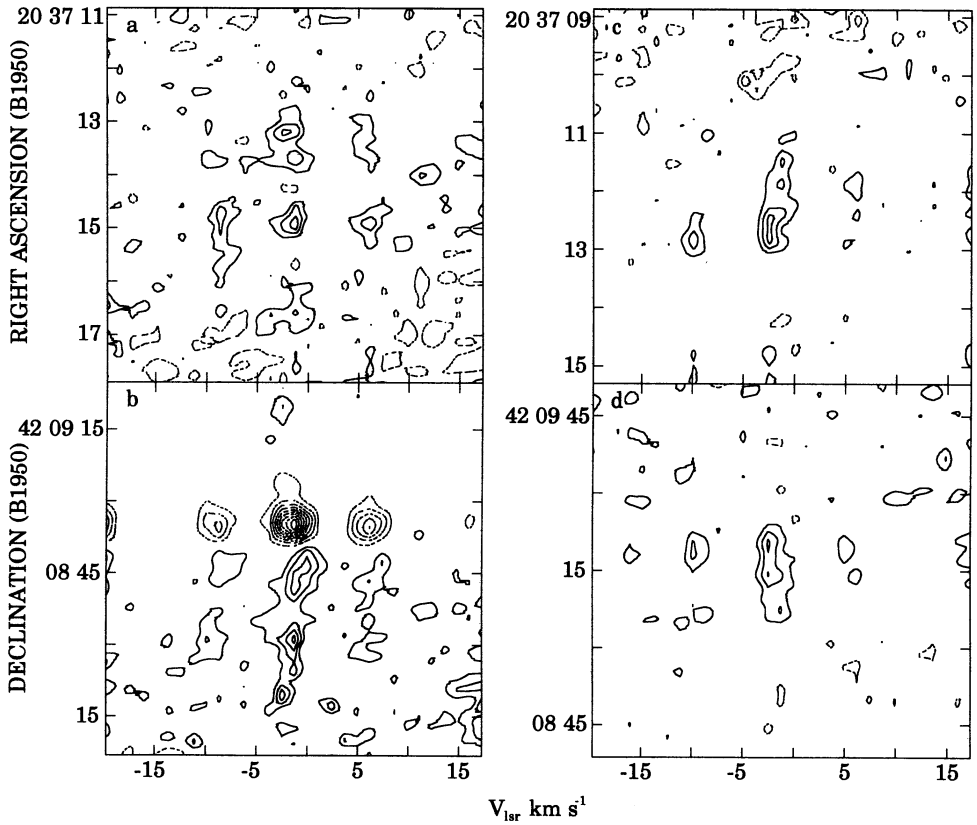

FIG. 4.—Beam-averaged position-velocity diagrams for the NH_3 (1, 1) regions studied by Keto (1990). The intervals for both emission (*solid lines*) and absorption (*dashed lines*) contours are 10 mJy beam^{-1} in Figs. 4*a* and 4*b* and 12.5 mJy beam^{-1} in Figs. 4*c* and 4*d*. The right ascension- and declination-v_{LSR} plots in Figs. 4*a* and 4*b* are for slices along decl. = 42°08′37″ and R.A. = $20^h37^m13^s.7$, respectively, and include NH_3 emission from regions 2, 3, and NH_3 absorption against the H II region. Figs. 4*c* and 4*d* are for slices along decl. = 42°09′14″ and R.A. = $20^h37^m12^s.4$, respectively, and include NH_3 emission from region 1.

Keto (1990), suggesting radial flow and collapse, are not easily seen in our plots. These features were found in the Keto (1990) data at low S/N levels. Above the 3 σ noise level there is excellent agreement between Keto (1990) and our higher spatial resolution and higher S/N data.

3.3. *The Distribution of Quiescent Dense Gas*

Much of the NH_3 emission in the DR 21 region is found in filamentary-like structures extended in a north-south direction. In contrast to the contracting cloud model of Keto (1990), the NH_3 filamentary morphology found for our data suggests a situation in which a dynamical interaction determines the structure of the molecular material. This may be caused by the roughly east-west outflow which has cleared out a path in the material close to DR 21, and we are observing the remaining material. To map the dense gas accurately, the (1, 1) line data are more appropriate. In this picture, the NH_3 is located in regions which have largely escaped being destroyed by the outflow. Compared to the virial masses from $C^{18}O$ (Wilson & Mauersberger 1990), it appears that only $\sim$10%–30% of the mass of the cloud near DR 21 is traced by the NH_3 (1, 1) line, the HCO^+, or HCN. The remaining 90% is not found in these more complex molecules. We believe that this underabundance of NH_3 and HCN may be the result of shock waves from the outflow, which dissociate these more fragile species, rather than excitation or measurement effects. This would be similar to the situation for Orion KL, where little NH_3 or HCN are present in the high-velocity outflow.

It is likely that the morphology of the NH_3 is caused by initial conditions. Then the NH_3 would be aligned north-south by magnetic fields in long filaments on scales of arcminutes. The effect of the outflow would be to clear out nearby material in its path, leaving NH_3 north and south of the flow direction. On a scale of a few arcminutes, the 6 cm H_2CO absorption mapped by Bieging et al. (1982) forms a filament-like region $>20'$ long, extending north-south, by $<5'$ east-west. About 15′ to the north, this filament curves to the west. The position angle of the NH_3 emission-line regions is rather similar to that of this large-scale distribution. Considering this remarkable alignment on these scales, the question arises as to the cause of the large-scale shape found for the DR 21 W75S cloud. If magnetic fields determine this structure, the ionization fraction must exceed 10^{-7}, and the *B* field strength must be of order 100 μG (see the discussion in Wilson & Mauersberger 1990). If so, the *B* field must extend over 20′ (from Bieging et al. 1982) and may have a helical structure, with the field lines wound around the cylinder of gas. The direction of this field would be approximately parallel to the galactic plane. The effect of this field on the energetic outflows would be small, but the rotation axes of the outflow source (or sources) may have been determined by the field. There may also be some residual effect of the initial configuration of the molecular material on the approximately north-south alignment of the NH_3 filaments. Unfortunately there is no information about direction or strength of the *B* field in this region. As discussed by Wilson & Mauersberger (1990), a possible alternative to an alignment by *B* fields is that

the molecular gas is swept up by the winds of stars located to the east and west of the cylinder. This possibility seems less likely, and the simplest explanation remains an alignment due to magnetic fields.

3.4. *The* NH_3 (3, 3) *Line Data*

Velocity-integrated intensities of the (3, 3) transition are shown in Figure 5*a*, and several regions of (3, 3) line emission are labeled. Continuum contours are shown as dashed lines in Figure 5*a*. Figures 5*b*–5*f* show contour plots of individual NH_3 (3, 3) velocity channels. To facilitate comparison to the (1, 1) emission and absorption, the panel size and region contoured in Figure 5 are identical to that used for Figure 2. The He81β recombination line is +0.46 MHz (−6 km s^{-1}) from the (3, 3) inversion line of NH_3 (the rest frequencies are to be found in Lilley & Palmer 1968 and Lovas 1991). However, when scaled

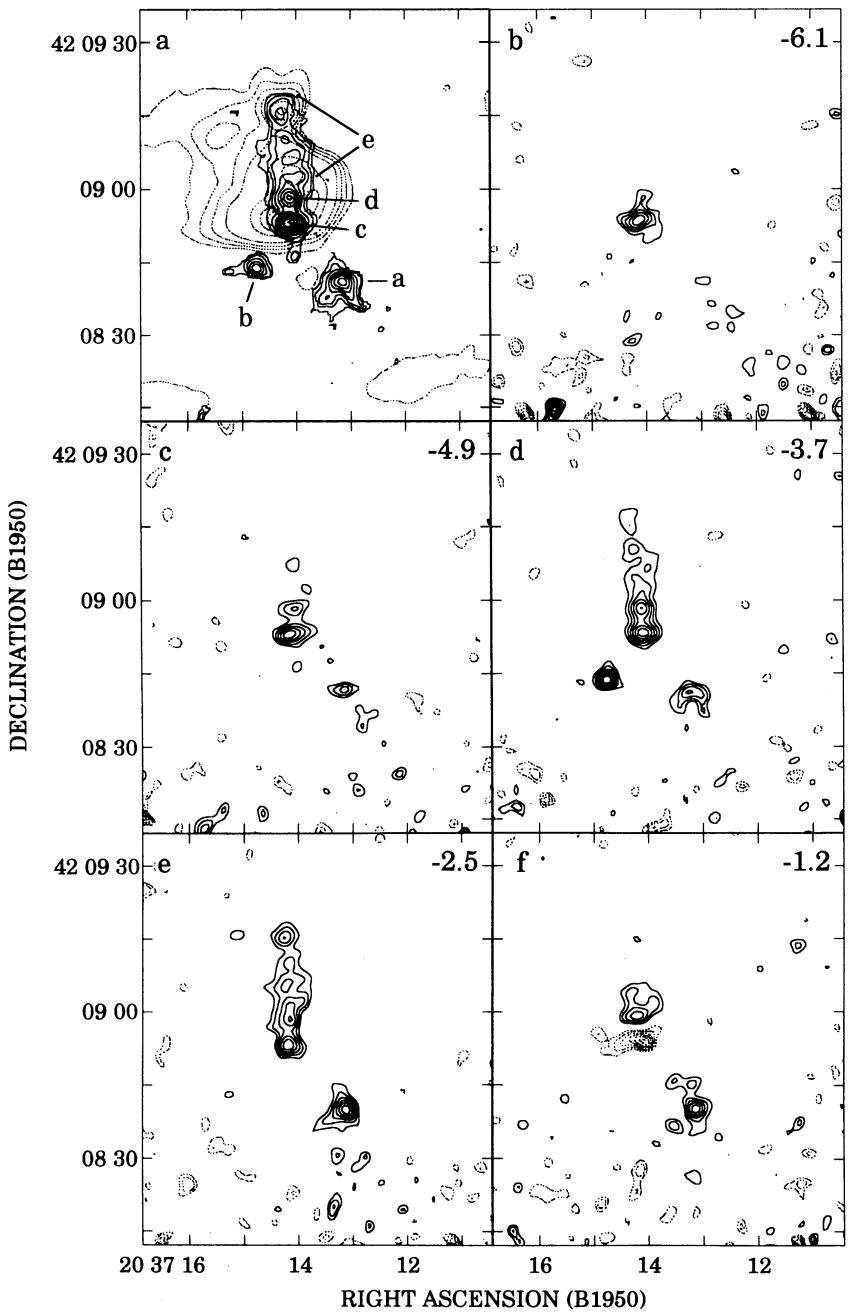

FIG. 5.—(*a*) Contour plot of the velocity-integrated NH_3 (3, 3) line intensities, integrated from −6.1 km s^{-1} to − 1.2 km s^{-1}. Contours of the continuum emission are shown as dashed lines. Spectra of the labeled regions (*a*–*e*) are shown in Fig. 6. Contours levels of the (3, 3) integrated line intensities are 10, 20, 30, 40, 50, 60, 70, 80, and 90% of 0.24 Jy beam^{-1} km s^{-1}. (*b*–*f*) Contour plots of the NH_3 (3, 3) emission and absorption in DR 21 for individual channels. The channel velocity, in km s^{-1}, is noted in the upper right-hand corner of each plot. The contour levels are −75, −65, −55, −45, −35, −25, 25, 35, 45, 55, 65, 75, and 85% of 89 mJy beam^{-1}. To facilitate comparison with the NH_3 (1, 1) emission and absorption, the location and size of each panel are identical to those used in Fig. 2. (*g*) Overlay of the integrated (1, 1) emission and absorption (*thin lines*) and the integrated (3, 3) emission (*thick lines*). The (1, 1) and (3, 3) contour levels are identical to those in Figs. 2*a* and 5*a*.

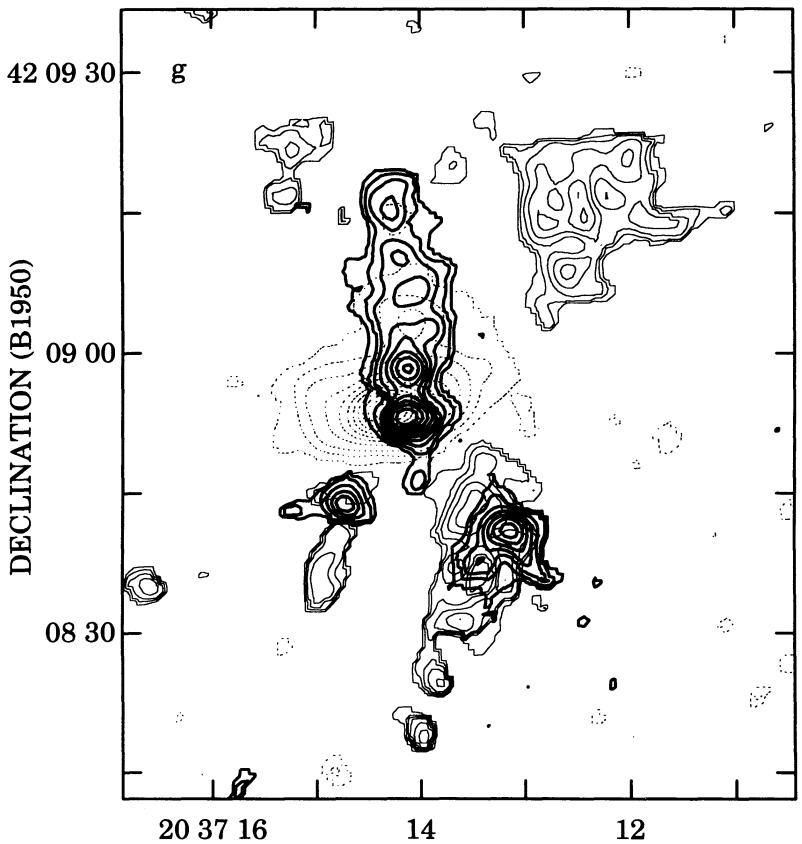

FIG. 5—*Continued*

from the LTE hydrogen-line intensity and the observed He/H ratio (Roelfsema et al. 1989), the He81β line will be 3×10^{-3} of the continuum intensity. This is below the level of the lowest contour shown in Figure 5. Thus, the line emission toward DR 21 is caused by the (3, 3) inversion line of NH_3, and not by the helium recombination line.

Compared to the NH_3 (1, 1) line, the (3, 3) line exhibits a wider velocity profile. The (3, 3) line is found predominantly in emission and is slightly blueshifted with respect to the (1, 1) line. These features are present in the single-dish NH_3 data of Guilloteau et al. (1983). The blueshifted line wing is found in rotationally excited OH spectra (Guilloteau et al. 1984). The spatial distribution of the (3, 3) NH_3 line is significantly different from that of the (1, 1) NH_3 line. Figure 5*g* shows the integrated (1, 1) emission and absorption (*thin lines*) overlaid on integrated (3, 3) emission (*thick lines*). Toward the continuum source, the (3, 3) emission is located in a filament that is extended north-south but compact east-west.

In the NH_3 (3, 3) line, at $v_{LSR} = -3.7$ km s^{-1}, there is a pointlike emission feature with a peak main beam brightness temperature of >40 K to the southeast of the continuum. We identify this as region b. To the southwest of the continuum, in region a, there is weaker, more extended emission. Projected onto the H II region is a filament-like structure, regions c, d, and e, oriented north-south, along with a weak absorption feature at $v_{LSR} = -1.2$ km s^{-1}. This prevalence of NH_3 (3, 3) emission toward the continuum region is very different from the (1, 1) line data, where only strong absorption is found. To analyze the (3, 3) emission and absorption line data further, we have produced spectra for the maxima identified in Figure 5*a*. These (3, 3) spatially integrated spectra are shown in Figure 6. The methods we employed follow those used to produce our (1, 1) line spectra, shown in Figure 3. Compared to the (1, 1) line data, our (3, 3) spectra are remarkably different. Presumably these differences are caused by molecular excitation and cloud structure. For regions a, c, d, and e, the (3, 3) profiles are markedly wider. The (3, 3) line arises from energy levels 100 K above the (1, 1) levels, so the (3, 3) emission must arise from warmer parts of the cloud closer to the heating sources. For example, NH_3 (1, 1) region 3 and NH_3 (3, 3) region a are spatially close, but the (3, 3) line has twice the width of the (1, 1) line, and the position of the (3, 3) maximum is nearer to the H II region. We surmise that the larger widths of the (3, 3) lines are caused by an interaction with the H II region and/or outflow source. This supposition is reinforced by the profile shapes for regions c and d (Fig. 6). In source c there is a noticeable absence of the emission toward positive v_{LSR}'s. This is probably not caused by a fortuitous canceling of emission by absorption, since an exact balance is unlikely. Instead, the narrower absorption may arise from a dense region of thermalized gas in front of the continuum source, where $T_{MB} = 400$ K. Region d is offset from the continuum maximum, and no absorption is found. We believe that the (3, 3) emission arises from higher excitation material closer to the boundaries of the H II region interacting with either outflows or ionized gas. Certainly for regions c and d, and possibly region a, the line widths cannot

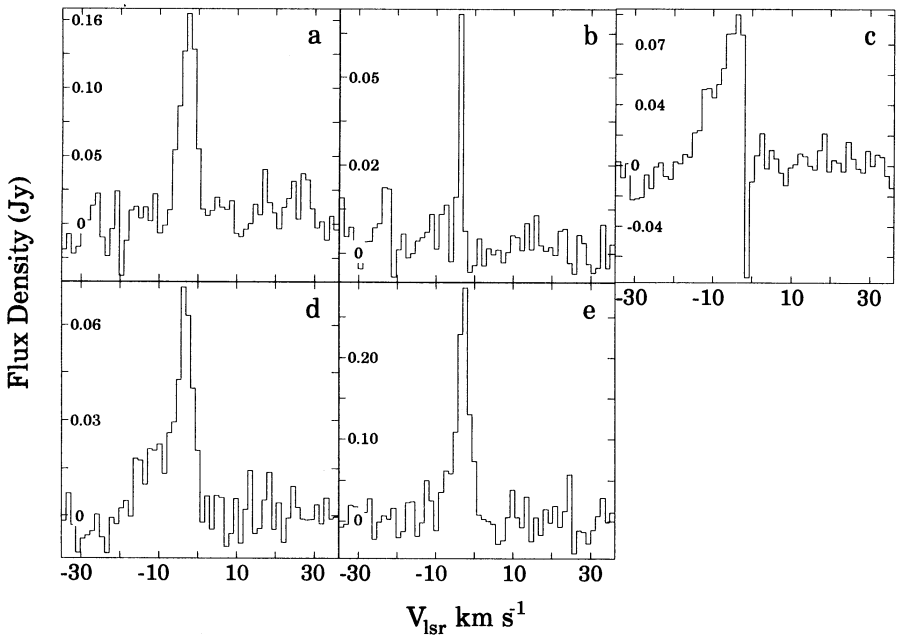

FIG. 6.—Spatially integrated spectra of the NH_3 (3, 3) inversion line toward emission-line regions a, b, c, d, and e (see Fig. 5*a*). The regions used for the spatial integrations were chosen from the zeroth-moment image (Fig. 5*a*).

be used to obtain virial masses. A comparison of the (1, 1) with the (3, 3) line profiles emphasizes the inhomogeneity of these molecular regions.

The peak single-dish flux density of the (3, 3) line is about twice that obtained from the VLA image. Some of the (3, 3) line emission must arise from extended, low surface brightness gas. This is particularly so for gas at positive radial velocities, since the negative velocity wing of the summed VLA (3, 3) profile is more intense than the positive velocity wing, but the single-dish profile appears to be nearly symmetric. If this positive v_{LSR} gas is spread out over a 1′ by 1′ region, the intensity in each beam is 2.5 mJy, about the lowest contour in Figure 5. We interpret the (1, 1) and (3, 3) line data as showing that the NH_3 clumps are mostly heated from the outside and that the (3, 3) lines arise from these hotter envelopes. The emission from region b is unresolved; maser action is the most likely process (see Gaume, Wilson, & Johnston 1995). If, as we suppose, regions c, d, and e are in front of the continuum source, the presence of emission is also an indication of maser emission. It is likely that inverted populations in the (3, 3) energy levels amplify the background continuum. The negative velocity wings seen toward regions c and d are also found in OH that is absorbing the radio continuum (Guilloteau et al. 1984). Thus, regions c and d are in front of the H II region. This negative velocity gas is not seen in the (1, 1) absorption, so it is presumably hot. In regions a and b, in Figure 5*a* the (3, 3) line optical depths must be ≥ 1 to give rise to maser emission since there is no background continuum. These must also be warm regions. A simplified account of the excitation is given by Guilloteau et al. (1983). The inversion is caused by a transfer of population in ortho–NH_3 from the $K = 0$ ladder to the $K = 3$ ladder. According to this excitation scheme, the densities must be about 10^5 cm^{-3}, similar to that found by Dickel et al. (1986) from H_2CO absorption-line studies toward DR 21. This density is about 3–4 times larger than the value obtained from the virial analysis of $C^{18}O$ data, but this merely indicates that the clouds are not uniform. The other possible explanation of the line emission toward DR 21 is that the (3, 3) line is hot and quasi-thermally excited. We feel that this is very unlikely, for two reasons. First, from single-dish data, the (4, 4) line emission is <0.05 of the (3, 3) emission. This is difficult to explain if there were a very hot molecular cloud producing the NH_3 (3, 3) emission toward the H II region (for data, see Wilson & Mauersberger 1990). Second, the velocity of the (3, 3) line is blueshifted. We interpret this as arising from hotter gas in front of the H II region being pushed in our direction. In summary, the simplest model to explain the characteristics of the (1, 1) and (3, 3) inversion line data toward the H II region involves weak maser emission from the (3, 3) line.

There is (3, 3) line emission but little (1, 1) line absorption toward the northern part of DR 21 (region e of Fig. 5*a*). We interpret this as an indication that T_k is larger toward the northern than toward the southern part of DR 21. This may be an explanation of the finding by Dickel et al. (1986) that the excitation is larger toward the north, from the ratios of 2 and 6 cm H_2CO absorption lines.

For the (1, 1) emission-zline regions 2 and 3, there are corresponding (3, 3) line features (see Fig. 5*g*). The lack of (3, 3) emission in (1, 1) emission-line regions 1 and 4 presumably indicates that T_k is lower in these regions. From HCN $J = 1$–0 line data, Dickel et al. (1985) concluded that the excitation is lower in region 1; since the HCN is optically thick, T_{ex} is smaller, that is, *either* lower density or lower T_k is responsible. From single-dish measurements of the (1, 1), (2, 2), and (4, 4) inversion lines of para–NH_3, Wilson & Mauersberger (1990) determined a value of $T_k = 65$ K. This single-dish value is the average over all of the emission-line regions. Our higher spatial resolution data show that the (3, 3) line is absent in the (1, 1) regions 1 and 4. This indicates a value of T_k lower than 65 K in these regions. A more exact determination of T_k is not possible,

since there may be deviations from the LTE value of the ortho to para ratio, in addition to the inversion of the (3, 3) inversion doublet level populations.

In summary, we believe that the larger line width observed in the (3, 3) inversion line is caused by an interaction of the hottest part of the molecular cloud with the shock front from the H II region and perhaps the outflow source. The (3, 3) emission arises in the warmer gas that is interacting with the expanding hot gas; the (3, 3) inversion level populations are slightly inverted and amplify a continuum background. Thus, the (3, 3) emission toward the H II region is biased toward foreground gas. This is not necessarily the case for all the NH_3 (3, 3) emission because components toward the southeast and southwest (regions a and b) are not projected onto the H II region. These must be extraordinary regions in which the optical depth in the (3, 3) inversion line is >1. We find that the (1, 1) emission and absorption represent the quiescent gas and that the (1, 1) line widths are appropriate for determining virial masses. The (3, 3) emission represents the interaction of molecular gas with outflows and the H II region. There may be deviations from LTE in the (3, 3) line emission.

3.5. *Interaction between the DR 21 Outflow and* NH_3 *Clouds?*

Since H II regions have already formed in the DR 21 complex, this source is probably somewhat older than W75S, 3′ to the north. We believe that a comparison with the Orion KL outflow is appropriate. The Orion KL outflow has a roughly east-west orientation and was identified with IRc2 (see, e.g., Genzel & Stutzki 1989). The outflowing gas is apparently moving at right angles to the line of sight because the HCO^+, CO, and vibrationally excited H_2 radial velocities in both the east and west lobes are within 20 km s^{-1} of the source velocity. From the outflow size (Garden & Carlstrom 1992, Fig. 3) and an assumed speed of 20 km s^{-1}, the DR 21 outflow started 3×10^4 yr ago. A lower age is possible if the outflow direction is closer to the plane of the sky. In contrast, the age of the Orion KL outflow is thought to be less than 10^4 yr. In the Orion KL source, the H_2O maser emission is vastly stronger than the emission in DR 21 and is spread over $\sim 30''$; at the distance of DR 21 this would be a size of about 12″. In contrast to Orion KL, there are no OH masers in the DR 21 complex. This lack of OH maser emission and the weaker H_2O maser emission may reflect either the greater age of the DR 21 source complex or the effect of the more powerful outflow; if there is greater turbulence, the maser amplification will be much lower. The energy and momentum in the DR 21 outflow are estimated to be up to 10 times that in the Orion KL outflow (see, e.g., Russell et al. 1992). Clearly, the source of this outflow must be extraordinary. The outflow source has not been identified so far, probably because of extinction even in the IR. We may be able to estimate the position of the outflow source from our NH_3 data. Toward the H II region, there are two (3, 3) line maxima, labeled c and d, in Figure 5, with prominent negative velocity line wings (Fig. 6). The emission may be caused by excitation effects, but the wings are certainly caused by kinematics. We assume that the negative velocity NH_3 is the result of an interaction with the outflow. We envisage the outflow as being mainly in a northeast-southwest direction, with only small amounts of gas being expelled in other directions. Toward us the molecular gas at the surface of dense clumps will have a negative radial velocity. The positive velocity component is not seen in NH_3 because this material is closer to the H II region and NH_3 is dissociated. The outflow source must be very close to either region c or d. For definiteness, we assume that the outflow source is located at the position halfway between regions c and d. This position is $\alpha = 20^h37^m14^s.1$, $\delta = +42°08'55''.6$ (B1950.0). We assume that the possible error is one-half the difference of these positions. On this basis, the error is 7″. The position we have identified for the outflow source is relatively close to the position of the H_2O maser (Genzel & Downes 1977). There may be a possible association of the outflow source with the H_2O maser, but the present positional accuracy is too low to give a quantitative estimate.

4. CONCLUSIONS

From 3″ images of the (1, 1) and (3, 3) inversion lines of NH_3 toward DR 21, we conclude the following:

1. There are molecular clouds seen in emission in the (1, 1) line southwest, south, northwest, and northeast of DR 21 and in absorption toward the continuum source. The (3, 3) line is seen mostly in emission, but there is some absorption. The (1, 1) line widths are ≤ 2.4 km s^{-1}, indicating quiescent gas. The (3, 3) lines are usually wider, asymmetric, and more blueshifted, indicating an interaction with the H II region and outflow source. The sharp falloff of continuum and the presence of dense molecular clouds indicates that the H II region is density bound to the southwest. There are no dense molecular clouds to the northeast, only low-brightness, extended continuum, so there the H II region is ionization bound.
2. The most massive clouds are southwest and northwest of DR 21 and have masses of about 100 $M_\odot$ from the (1, 1) line data. This is only about 10% of the total mass of the molecular cloud associated with DR 21. The cloud in the southwest shows a rotation-like motion, with a gradient of about 15 km s^{-1} pc^{-1}.
3. The positions of the southwest emission-line cloud and the absorption-line region indicate a physical connection between the two.
4. The emission-line cloud toward the northwest part of DR 21 is cooler than the clouds toward the south and southwest; probably T_k is <50 K for the northwest cloud, while for the south and southwest clouds, T_k is >65 K.
5. The filamentary structure of the emission-line clouds indicates a dynamical interaction with the powerful outflow from DR 21. There is good evidence for this from the (3, 3) line data. The position angles of these structures are nearly the same as found for the DR 21 W75S region.
6. The different widths, spatial distributions, and shapes of the (1, 1) and (3, 3) lines show that the molecular clouds are very inhomogeneous. Most of the (3, 3) line emission must arise near the regions at which the H II gas and/or outflow disturbs the molecular gas.
7. The NH_3 (3, 3) regions with prominent negative velocity line wings, regions c and d, show that this outflowing gas is in front of the H II region. These NH_3 (3, 3) emission regions are likely those closest to the outflow, and if the outflow source is midway between these regions, then it is located near $\alpha = 20^h37^m14^s.1$, $\delta = +42°08'55''.6$ (B1950.0). This is reasonably close to the H_2O maser near DR 21.

Basic research in Radio Interferometry at the Naval Research Laboratory is supported by the Office of Naval Research. T. L. W., K. J. J., and A. R. T. were supported in part

by the Max-Planck-Forschungspreis, administered by the A. von Humboldt-Stiftung. A. R. T.'s stay at NRL and USNO is supported in part by an HSP II grant from the Deutsche Akademische Austausch Dienst. We thank J. Fisher and J. Martín-Pintado, and especially E. Keto and C. M. Walmsley, for useful discussions.

REFERENCES

Bieging, J., Wilson, T. L., & Downes, D. 1982, A&A., 49, 607
Cornwell, T. J., Uson, J. M., & Haddad, N. 1992, A&A, 258, 583
Danby, G., Flower, D. R., Valiron,P., Schilke, P., & Walmsley, C. M. 1988, MNRAS, 235, 229
Dickel, H. R., Goss, W. M., Rots, A. H., & Blount, H. M. 1986, A&A, 162, 221
Dickel, H. R., Ho, P. T. P., & Wright, M. C. H. 1985, ApJ, 290, 256
Fisher, J., Sanders, D. B., Simon, M., & Solomon, P. M. 1985, ApJ, 293, 508
Garden, R., & Carlstrom, J. E. 1992, ApJ, 392, 602
Garden, R., Geballe, T. R., Gatley, I., & Nadeau, D. 1986, MNRAS, 220, 203
Gaume, R. A., Wilson, T. L., & Johnston, K. J. 1995, in preparation
Genzel, R., & Downes, D. 1977, A&AS, 30, 145
Genzel, R., & Stutzki, J. 1989, AR&A, 27, 41
Guilloteau, S., Baudry, A., Walmsley, C. M., Wilson, T. L., & Winnberg, A. 1984, A&A, 131, 45
Guilloteau, S., Wilson, T. L., Martin, R. N., Batrla, W., & Pauls, T. A. 1983, A&A, 124, 322
Harris, S. 1973, MNRAS, 162, 5P
Keto E. R. 1990, ApJ, 350, 722
Lilley, A. E., & Palmer, P. 1968, ApJS, 16, 143
Lovas, F. J. 1991, J. Chem. Phys. Ref. Data, 21, 181
Matsakis, D., et al. 1977, ApJ, 214, L67
Matsakis, D., et al. 1981, ApJ, 250, L85
Mauersberger, R., Wilson, T. L., Mezger, P. G., Gaume, R., & Johnston, K. J. 1992, A&A, 256, 640
Morris, M., Palmer, P., Turner, B. E., & Zuckerman, B. 1974, ApJ, 191, 349
Righini-Cohen, G., Simon, M., & Young, E. T. 1979, ApJ, 232, 782
Roelfsema, P. R., Goss, W. M., & Geballe, T. R. 1989, A&A, 222, 247
Russell, A. P. G., Bally, J., Padman, R., & Hills, R. E. 1992, ApJ, 387, 219
Wilson, T. L., Batrla, W., & Pauls, T. A. 1982 A&A, 110, L20
Wilson, T. L., Bieging, J. H., & Wilson, W. E. 1979, A&A, 71, 205
Wilson, T. L., & Mauersberger, R. 1990, A&A, 239, 305